Bulletin of the Seismological Society of America, Vol. 101, No. 3, pp. 1039–1054, June 2011, doi: 10.1785/0120090322

Probabilistic Seismic-Hazard Assessment Including Site Effects for Evansville, Indiana, and the Surrounding Region

by Jennifer S. Haase, Yoon Seok Choi, Tim Bowling, and Robert L. Nowack

Abstract Evansville, Indiana, is one of the closest large urban areas to both the New Madrid Seismic Zone, where large earthquakes occurred in 1811–1812, and the Wabash Valley Seismic Zone, where there is evidence of several large prehistoric earthquakes in the last 14,000 yr. For this reason, Evansville has been targeted as a priority region for urban seismic-hazard assessment. The probabilistic seismic-hazard methodology used for the Evansville region incorporates new information from recent surficial geologic mapping efforts, as well as information on the depth and properties of near-surface soils and their associated uncertainties. The probabilistic seismic-hazard calculation applied here follows the method used for the 2008 United States Geological Survey (USGS) national seismic-hazard maps, with modifications to incorporate estimates of local site conditions and their uncertainties, in a completely probabilistic manner. The resulting analysis shows strong local variations of acceleration with 2% probability of exceedance in 50 yr, which are clearly correlated with variations in the thickness of unconsolidated soils above bedrock. Spectral accelerations at 0.2-s period range from 0.6 to 1.5g, values that are much greater than those of the USGS national seismic-hazard map, which assume B/C site conditions with an average shear-wave velocity of 760 m/s in the top 30 m. The presence of an ancient bedrock valley underlying the current Ohio River flood plain strongly affects the spatial pattern of accelerations. For 1.0-s spectral acceleration, ground motions are significantly amplified due to deeper soils within this structure, to a level comparable to that predicted by the national seismic-hazard maps with D site conditions assumed. For PGA and 0.2-s spectral acceleration, ground motions are significantly amplified outside this structure, above the levels predicted by the national seismic-hazard maps with uniform D site conditions assumed.

Introduction

The three large New Madrid earthquakes that occurred in 1811–1812 generated ground shaking throughout the central and eastern U.S. Moment magnitudes (M_w) ranging from 7.4 to 8.1 have been assigned to the largest of the events based on intensity reports (Johnston, 1996; Hough *et al.*, 2000; Bakun and Hopper, 2004). In southwestern Indiana, the reported intensities ranged from modified Mercalli intensity (MMI) VI to VII (Nuttli, 1973; Street, 1984). A recurrence of a New Madrid–type event of this size is of concern in regional urban areas such as Evansville, Indiana (population 120,000), where earthquake damage could occur.

The United States Geological Survey (USGS) has carried out a probabilistic analysis of earthquake hazard for the U.S. (Frankel *et al.*, 1996; Frankel *et al.*, 2002; Petersen *et al.*, 2008). Earthquakes from all possible regional seismic sources, each with a given probability of occurrence, are taken into account for this analysis. This includes random sources, whose probability of occurrence is determined from gridded estimates of Gutenberg–Richter seismicity rates valid for the observed regional background seismicity (Richter, 1958; Weichert, 1980), as well as characteristic earthquake sources along known faults with estimated recurrence rates. The ground-motion levels likely to be observed from the seismic sources are specified in a suite of attenuation relations (Table 1), along with their associated uncertainties. A hazard curve is constructed at each site in the gridded map area that gives the probability of a certain ground-motion level being exceeded, given the probability of occurrence of each seismic source and the probability of observing a given ground-motion level at the appropriate distance from that source. The ground motion corresponding to a prescribed probability level of exceedance is selected from the hazard curve at each site in the area of interest to make a probabilistic seismic-hazard analysis (PSHA) map. The USGS produced national seismic-hazard maps for the central and eastern U.S. in 1996 (Frankel *et al.*, 1996), with updates

Table 1
Attenuation Relationships and Their Associated Weight Used in the Probabilistic Ground Motion Calculations

Attenuation Curve Reference	Weight
Toro *et al.* (1997)	0.2
Frankel *et al.* (1996)	0.1
Campbell and Bozorgnia (2003)	0.1
Atkinson and Boore (2006); 140 bar stress drop	0.1
Atkinson and Boore (2006); 200 bar stress drop	0.1
Tavakoli and Pezeshk (2005)	0.1
Silva *et al.* (2002)	0.1
Somerville *et al.* (2001)	0.2

in 2002 (Frankel *et al.*, 2002), and most recently in 2008 (Petersen *et al.*, 2008).

For the central and eastern U.S., the seismicity-derived hazard component is based on a catalog of earthquakes with magnitude 3.0 or greater from 1700 through 2006. The size of the largest possible earthquake is M_w 6.6 to 7.2 within the central and eastern parts of the North American continent outside specific seismic zones such as the eastern Tennessee, New Madrid, and Wabash Valley Seismic Zones and M_w 7.1 to 7.7 for the extended continental margin. The Wabash Valley region is assigned a maximum magnitude of M_w 7.5. The relatively high maximum magnitude assigned for the Wabash Valley is supported by paleoliquefaction evidence from six past earthquakes of $M_w > 6.0$ in southern Indiana and Illinois (Munson *et al.*, 1995; Munson and Munson, 1996; Pond, 1996; McNulty and Obermeier, 1999; Wheeler and Cramer, 2002; Green *et al.*, 2005; Olson *et al.*, 2005), including one earthquake near Vincennes about 6100 yr ago that may have been as large as M 7.5 (Munson *et al.*, 1995; Green *et al.*, 2005). The characteristic earthquake-derived component of the seismic hazard in the central and eastern U.S. (CEUS) is based on four finite source areas where paleoseismic data constrain recurrence rates: New Madrid, Missouri; Charleston, South Carolina; Meers, Oklahoma; and Cheraw, Colorado. Because of the uncertainty in recurrence rates and earthquake magnitude, several weighted estimates of the seismic hazard are combined. Several cases are considered for the New Madrid source region, which is the closest and most important of the characteristic earthquake sources. The seismic source size is varied from M_w 7.1 to 8.0, the location of the New Madrid rupture is varied among five possible locations of the three fault branches that ruptured in 1811 and 1812, and clustered and unclustered models are considered. Given some uncertainty on the completeness of the record between 1450 and 2350 B.C., the recurrence interval for a New Madrid–type of event has been estimated to be 500 to 1000 yr (Tuttle *et al.*, 2002; Tuttle *et al.*, 2005). However, low rates of deformation observed by GPS in the midcontinent indicate that present-day recurrence rates may be lower or that the deformation is not steady over time (Calais and Stein, 2009). Currently, recurrence interval estimates of 500 to 750, 1000, and 1500 yr have been retained for the estimation of probabilistic seismic hazard in the 2008 USGS national seismic-hazard maps (Petersen *et al.*, 2008), and that approach is followed here. Seven attenuation curves (Table 1) are used that assume standard National Earthquake Hazards Reduction Program (NEHRP) B/C site conditions (Building Seismic Safety Council, 2003), which implies shear-wave velocities of 760 m/s in the top 30 m of the soil at a given site. The hazard calculation takes into account random variations in ground motion using the uncertainty assigned to the attenuation curves. The probabilistic seismic-hazard maps take into account source uncertainties through a logic-tree approach of varying the different source parameters. The relative contribution of distributed sources, such as the Wabash Valley Seismic Zone (WVSZ), compared to characteristic earthquake sources, such as the New Madrid Seismic Zone (NMSZ), is established using relative weighting of the resulting hazard curves for each type of source model. Figure 1 shows for Indiana the calculated peak ground acceleration (PGA) and spectral acceleration at 0.2-s and 1.0-s periods

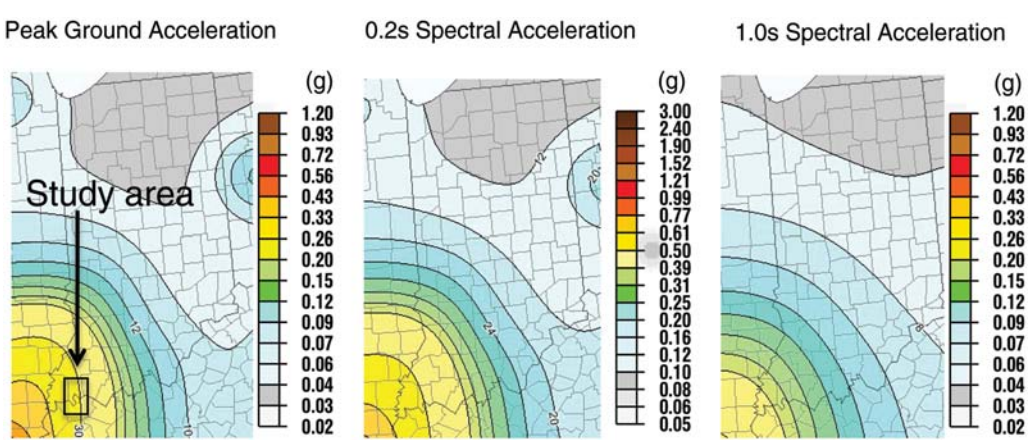

Figure 1. 2008 USGS national seismic-hazard map shown for the Indiana region for 2% probability of exceedance in 50 yr at (left) PGA, (middle) 0.2-s spectral acceleration, and (right) 1-s spectral acceleration (Petersen *et al.*, 2008). By default, the maps include the site response for a NEHRP B/C site classification. Rectangle in the left map shows the Evansville study region.

with 2% probability of exceedance (PE) in 50 yr from the 2008 USGS national seismic-hazard maps. Further details on the PSHA methodology can be found in the documentation for the national seismic-hazard maps and other literature (Frankel *et al.*, 1996; Frankel *et al.*, 2002; McGuire, 2004; Petersen *et al.*, 2008).

Current USGS probabilistic seismic-hazard estimates show higher seismic hazard in southwestern Indiana than for the rest of Indiana, primarily due to the proximity of the New Madrid Seismic Zone. However, local geology and soil conditions influence the characteristics of ground motion in terms of amplitude, frequency content, and duration (Kramer, 1996). The effect of local site conditions on ground motion is not considered in the USGS national seismic-hazard maps. These maps assume a default firm rock site response with NEHRP B/C site conditions.

The objective of this work is to produce a probabilistic seismic-hazard map for the nine-quadrangle region surrounding Evansville that takes into account ground-motion amplification due to near-surface geologic materials. The depositional history of the area includes several periods of glacier advance and retreat, leaving behind sequences of till and loess, periods of slackwater lake deposition, and recurring sequences of fluvial deposition and overbank deposits in the Ohio River valley. The near-surface soils are expected to have a major impact on the ground-motion amplification in the probabilistic seismic-hazard calculation. The Data section describes the data used to develop a three-dimensional (3D) model for soil properties and bedrock depth necessary for site effect calculations. Analysis of Local Geology and CPT Sounding Data describes the method used for creating the 3D near-surface shear-wave velocity model. Bedrock Depth describes the method for creating the bedrock depth model. Site-Amplification Calculation describes the seismic amplification calculated using this 3D model. Probabilistic Seismic-Hazard Calculation and Results describes the resulting probabilistic seismic-hazard maps and provides a discussion comparing them to the USGS national seismic-hazard maps, and the conclusions are summarized in the Conclusions section.

Data

Subsurface information on soil properties is required for the site-amplification analysis. Parameters significantly affecting the site response calculation are the bedrock depth, shear-wave velocity, soil type, density, and the dynamic properties (shear modulus reduction and damping curves) of the soil column. Most of these parameters can be determined from field site investigations. Two parameters, the depth-to-bedrock and the shear-wave velocity of soil layers, are the most important in terms of determining the seismic amplitude. Because it is not feasible to collect data at all points in the study region, we develop several reference models from the observed data. Geology provides a context for generalizing incomplete and sparse geophysical data. This study takes advantage of recent surface geologic mapping and a compilation of new and existing subsurface test data to develop such a model.

Geologic Setting and Map

The surficial geology along the Ohio River valley near Evansville consists of glacial and interglacial lithologic sequences characterized by a series of fluvial and lake depositional events, in which relatively thick Ohio River fluvial deposits backed up tributary streams to form lakes (Eggert *et al.*, 1996, 1997a,b). The geologic maps are used to associate representative shear-wave velocity profiles with regions of similar depositional history and properties. The geologic mapping was carried out through a collaboration called the Evansville Area Earthquake Hazards Mapping Project, with contributions from the Indiana Geological Survey (IGS), the Kentucky Geological Survey (KGS), and the USGS. The surficial geology was mapped in 24 different units at a 1:50,000 scale for seven and a half of the nine quadrangles in the study region (Fig. 2; Moore *et al.*, 2009). Although not all of these units are distinct seismically, they provide a context for generalizing seismic properties for a simplified model. For the remaining area in the northwest quadrangle and half of the northeast quadrangle, the most recently available quaternary geologic map at a 1:500,000 scale was used (Gray, 1989). In these quadrangles, the lower resolution is not critical, because much of these two quads consists of bedrock covered by thin loess, and the few alluvial units present are reasonably well represented even with this lower resolution. Strip mined areas are not considered in this study, The geologic units of the two different scale maps were correlated, and the unit designations were taken from the 1:50,000 scale maps.

Subsurface Data

The available subsurface geotechnical data sets inside the nine-quadrangle study area include water well logs, *in-situ* soil profiles using the cone penetration test (CPT) with shear-wave measurements and standard penetration test (SPT), down-hole shear-wave velocity tests, and seismic refraction profiles (Table 2). Fifty-two CPT soundings were made on the Indiana side of the Ohio River and six CPT soundings were made on the Kentucky side (Holzer, 2003). These CPT measurements contain tip resistance, sleeve friction, and *S*-wave travel time. *S*-wave velocity and soil type can also be inferred from these measurements. The CPT data set was the primary data set used for establishing reference *S*-wave velocity profiles to depths of 20 m. The IGS compiled 570 SPT boring logs from 59 sites (Y.-S. Choi and J. Hill, personal commun., 2005). The blow-count data at these sites provided shallow bedrock depth information, which was incorporated into the bedrock surface model. Twenty-six borehole *S*-wave velocity profiles and soil type logs were also compiled (Eggert *et al.*, 1994). These were used for independent verification of the accuracy assigned to the

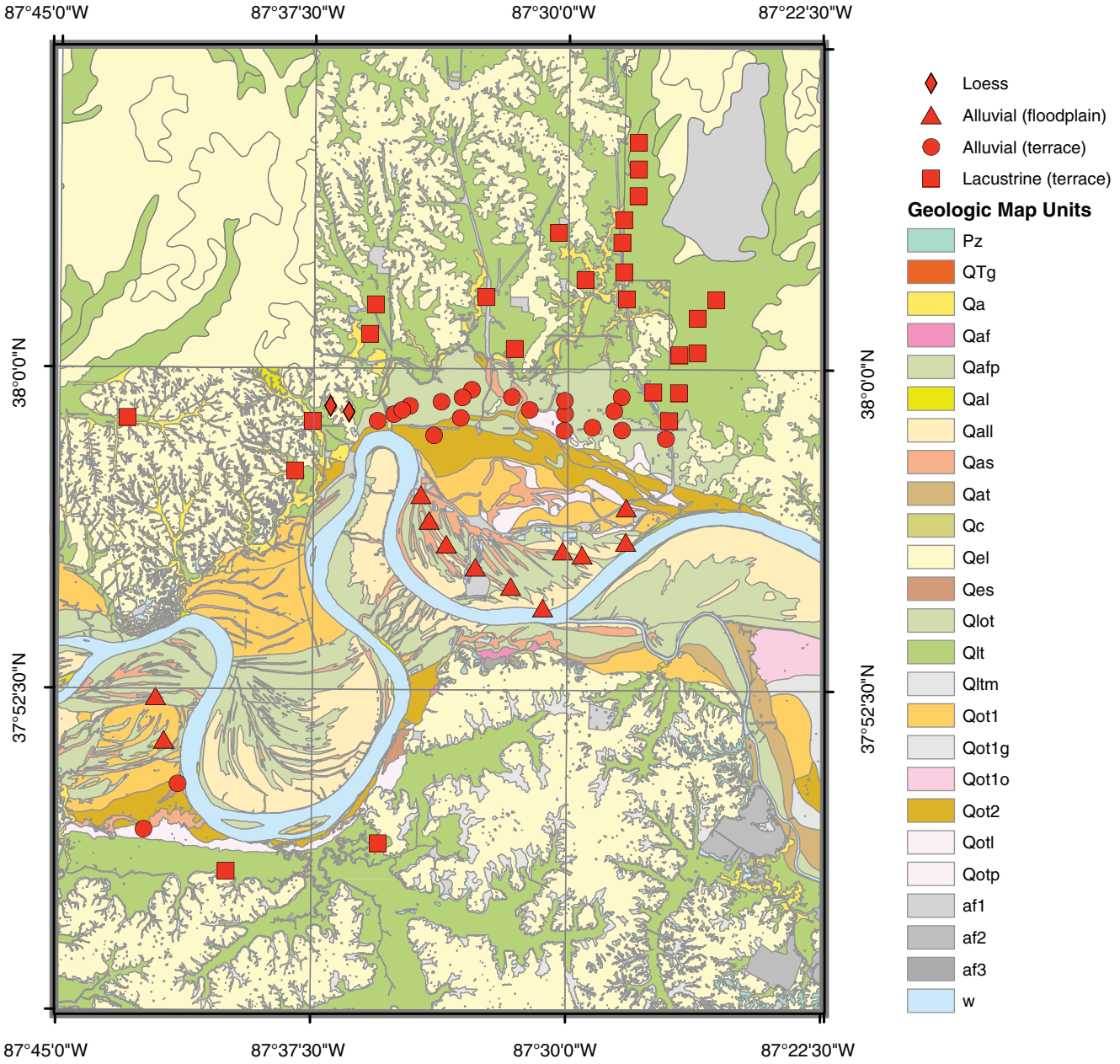

Figure 2. Merged geologic map from the 1:50,000 (Moore *et al.*, 2009) and 1:500,000 (Gray, 1989) scale maps. Mapped units are Qc: Colluvium, Qal: Alluvium, Qall—: Levee deposit alluvium, Qas: Alluvium in modern floodplain sloughs, Qaf: alluvium in alluvial fans, Qafp: River floodplain alluvium, Qat: Low terrace alluvium, Qa: Creek and sheetwash alluvium, Qes: Dune sand, Qel: Loess, Qot1o: Reworked Ohio River terrace outwash alluvium, Qot1g: Reworked Green River terrace alluvium, Qltm: Upland marginal lacustrine deposits, Qlt: Lacustrine terrace slackwater deposits, Qot1: Low terrace outwash alluvium, Qlot: Lacustrine and outwash terrace deposits, Qotp: Paleolevee deposits on outwash terrace, Qot2: High terrace outwash alluvium, QTg: Upland gravel, Pz: Paleozoic bedrock, w: Surface water, af1,af2,af3: Artificial fill. See Moore *et al.* (2009) for a detailed description of surficial geologic units. Red symbols indicate locations of CPT profiles.

reference velocity profiles above 20 m depth and were used for determining the velocity profiles below 20 m depth. In addition, the IGS database of 228 *P*-wave refraction profiles (Rudman *et al.*, 1973) was used to provide observations of bedrock depth. A series of 15 *S*-wave refraction profiles (CUSEC, 2004) in and around Evansville provide checks on the characteristic velocities for the soil types and also provide shear-wave velocity for bedrock. The IGS iLITH database of 827 water well logs provided additional data on the bedrock depth and provided information on the soil type profile with depth (Bleuer, 2000). Five-hundred eighty-three bedrock elevations from KGS coal, oil, gas, and water well logs (R. Counts, KGS, personal commun., 2005) are available on the Kentucky side of the Ohio River as well. The locations of all the subsurface data are shown in Figure 3.

Table 2
Descriptions of Subsurface Observations Available in the Evansville Region

Data Type	Reference
58 CPT profile data collected by the USGS	Holzer (2003)
26 borehole *S*-wave velocity profiles	Eggert *et al.* (1994)
570 SPT blow count data at 59 geotechnical boring sites	(Y.-S. Choi and J. Hill, personal commun., 2005)
228 *P*-wave seismic refraction profiles	Rudman *et al.* (1973)
15 nearby *S*-wave refraction profiles	CUSEC (2004)
Indiana Geological Survey iLITH GIS database of approximately 827 water well logs	Bleuer (2000)
583 Kentucky Geological Survey oil, gas, water well logs	(R. Counts, personal commun., 2005)

Analysis of Local Geology and CPT Sounding Data

The CPT profiles have been grouped by soil characteristics in order to derive general shear-wave velocity model profiles for each type of depositional environment. The geologic units described predominantly as river alluvium (Fig. 4, lower left profiles) typically have varying thicknessses of silty clay to sandy silt overlying more extensive thicknesses of sand and gravel. Soil profiles located within geologic map units that are considered outwash terrace deposits and mixed overbank with interfingered lacustrine deposits (Fig. 4, upper left profiles) typically have alternating layers of silty clay to silty sand of varying thickness. For the soil profiles that are located within surficial geologic map units that are described as lacustrine, clay is the dominant soil type, as shown on the upper and lower right in Figure 4. There are no CPT soundings located within the geologic map units that are described as loess; however, two of the borehole shear-wave velocity measurements were made in these units.

For the CPT soundings belonging to the river alluvium group, the average shear-wave velocity was calculated at each 2-m depth interval from the CPT shear-wave velocity measurements to a depth of 20 m. There were 7–12 measurements available at each interval to contribute to these averages. These values were verified with similar averages made from the borehole shear-wave measurements that were made in these units (Eggert *et al.*, 1994) and agreed much better than the uncertainty in the borehole shear-wave velocity, except in the first layer. Similarly, for the CPT soundings belonging to the Outwash Terrace group, 20 to 21 measurements were available at each 2-m interval to contribute to the average shear-wave velocity profile to a depth of 20 m. For the lacustrine terrace group, 12 to 25 measurements were available at each 2-m interval to contribute to the average shear-wave velocity profile to a depth of 20 m. There was only one CPT sounding that extended to 30 m in the river alluvium group and one CPT sounding that extended to 30 m in the lacustrine terrace group; however, there were eight borehole shear-wave profiles that extended to 35 m. Therefore, all of the available borehole shear-wave profiles were used to calculate the average velocity from 20 to 30 m depth at 2-m intervals and to calculate the average velocity from 30 to 40 m depth at 4-m intervals. This assured that more than eight measurements contributed to each interval average. The one available 30-m CPT sounding in the river alluvium group and the one available CPT sounding in the lacustrine terrace group agreed with the borehole shear-wave velocity averages to within one standard deviation. Therefore, the average borehole shear-wave velocity profile was used for all groups for depths greater than 20 m. For the loess and colluvium group, the only two available borehole shear-wave velocity measurements were used to calculate average velocities at 2-m intervals to a depth of 10 m.

The average velocity and the standard deviation of the velocity at each depth for the three groups are shown in Figure 5 and listed in Table 3. The standard deviation of the differences between all of the individually observed layer velocities and the average layer velocities is 63.9 m/s. The uncertainty for each velocity at each depth is also listed in Table 3 and is equally as important as the velocity value because it determines the range of variations that are simulated in the site-amplification analysis to determine the uncertainty in the site amplification. Note that there is not a large range of velocities present for the soils among the reference velocity models, so the variations in bedrock depth are likely to play a more important role than soil type in the final amplification calculation.

Each grid point in the study area is then assigned one of the four velocity profiles based on its location. This yields the geographic distribution of reference velocity profiles shown in Figure 6. At each site, the appropriate reference model velocities are used above the bedrock depth at that point, and the bedrock velocity is used below that depth.

Bedrock Depth

Previously mapped bedrock elevation contours at a 1:500,000 scale (Gray, 1983) are not detailed enough to capture smaller scale variability of the bedrock surface that controls site amplification. Development of a detailed model for bedrock depth based on all available data is required to calculate the site response. The compiled depth observations from SPT measurements, oil, gas, and water well logs, and *P*-wave refraction measurements were used to determine a model for the bedrock depth. At each available data point, the bedrock elevation was calculated by subtracting the bedrock depth from the USGS 1 arcsecond digital elevation model (DEM) raster value at the point location (USGS, 2004). Points were included beyond the nine-quadrangle area of interest to avoid edge effects in the interpolation.

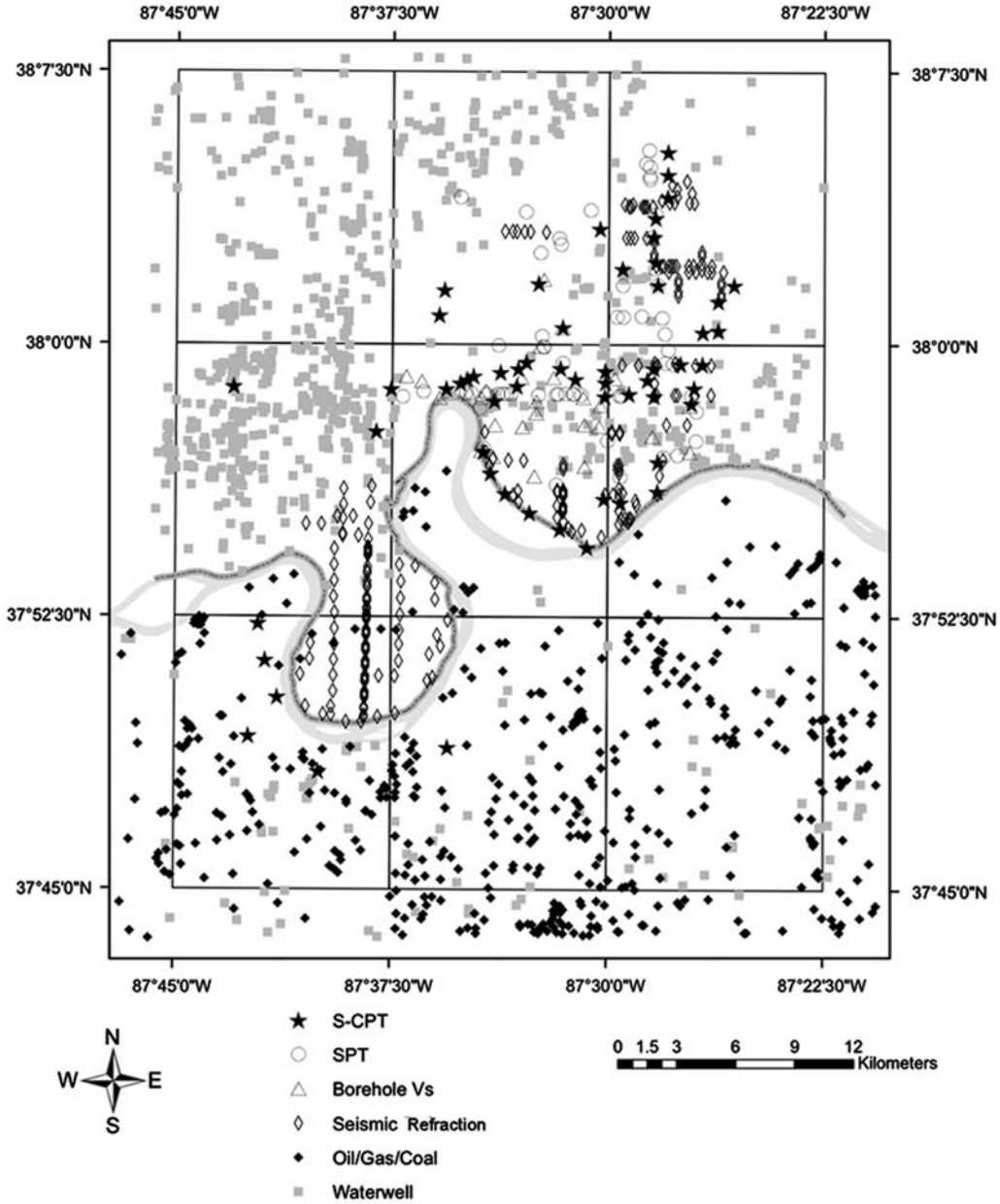

Figure 3. Locations of subsurface observations used in the Evansville region.

Several steps were combined in the process to interpolate the point data to construct an optimal gridded bedrock depth model. The uplands within the study area are primarily loess-covered bedrock. As the loess was deposited, it formed a blanket of eolian sand and silt that gradually increases in thickness from the northeast to the southwest. Because the loess surface mimics the bedrock surface, the bedrock depth (soil thickness) is interpolated rather than bedrock elevation. In that way, a smoothly interpolated bedrock depth model that has limited spatial resolution actually results in a bedrock elevation model with comparable roughness to that of the surface. On the other hand, in the lowlands regions where the current surface topography is a result of river processes and is not directly dependent on the bedrock elevation, we smoothly interpolate the bedrock elevation data points so that the complexity of the bedrock surface realistically reflects the resolution of the data density. The uplands model and lowlands model are merged at the 110 m above sea level (ASL) bedrock elevation contour level, which corresponds very closely to the location of the edge of the ancient bedrock valley walls. The resulting bedrock depth and bedrock elevation maps are shown in Figure 7. The standard deviation of the difference between the data points and the model surface is 1.2 m in the uplands and 3.7 m in the lowlands. This uncertainty is also important in determining the range of variation in the site response calculated at each point. At several point locations, where detailed independent information was available (i.e., at the Advanced National Seismic System [ANSS] seismic station site, the Pigeon Creek geotechnical site, and a refraction profile location), the bedrock surface

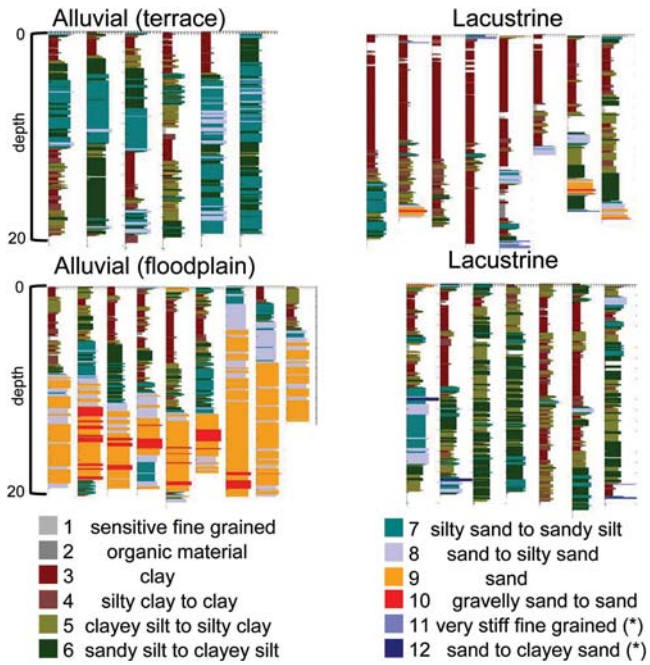

Figure 4. Soil profiles from the CPT data from the alluvial group in the terrace and floodplain locations (left) and lacustrine group (right) (profiles are reproduced from Holzer [2003]. The alluvial group includes profiles in both the terrace and floodplain.

did fall within the two standard deviations of the bedrock elevation model at those points.

The bedrock depth is greatest within the ancient bedrock valley underlying the current Ohio River floodplain, where the surface is categorized primarily as different types of alluvium and outwash deposits on the surficial geologic map (Fig. 2). The bedrock depth is as great as 50 m close to the Ohio River, with very steep valley walls in the ancient bedrock topography at depth. In contrast, bedrock depth in the northern or southern upland areas is relatively shallow, usually less than 13 m, reflecting the varying thickness of overlying loess or colluvium. There are large changes in soil thickness at the edges of the river valley.

Site-Amplification Calculation

The variation of bedrock depth and the shear-wave velocity in the soil and bedrock are the primary parameters influencing site amplification. An approximate map of the resonant period at each grid point was calculated to give a preliminary indication of how site-amplification maps and probabilistic hazard maps are expected to vary spatially as a function of period. At each point, the appropriate reference model velocities are averaged over depth from the specific bedrock depth at the site to the surface using a weighted average based on travel time in the layers. An estimate of the fundamental period was calculated at each point within the study area using the approximate relation

$$T = \frac{4d}{\bar{V}_s},$$

where d is depth and $\bar{V}_s$ is the depth-averaged shear-wave velocity.

While the use of this formula is not accurate enough for the final seismic-hazard products, from this simplified calculation, the amplification within the floodplain is evident for periods near 1.0 s (Fig. 8). The amplification at a resonance near 0.2 s shows up at the edges of the floodplains, where the sediments are approximately 5–15 m thick.

Site effects are often accounted for by multiplying the spectral accelerations determined from the PSHA for rock conditions by site response coefficients. However, these coefficients do not account for the uncertainty in the soil properties. The PSHA calculation considers uncertainties in source and attenuation, so it should also take into account the uncertainty in the knowledge of the amplification factor and the uncertainty in the profile properties from which the amplification was derived. Otherwise, this type of calculation is not completely probabilistic. The methodology developed for a completely probabilistic calculation incorporating site effects (Cramer, 2003) has been successfully applied to the Memphis area (Cramer *et al.*, 2004). In the Memphis study,

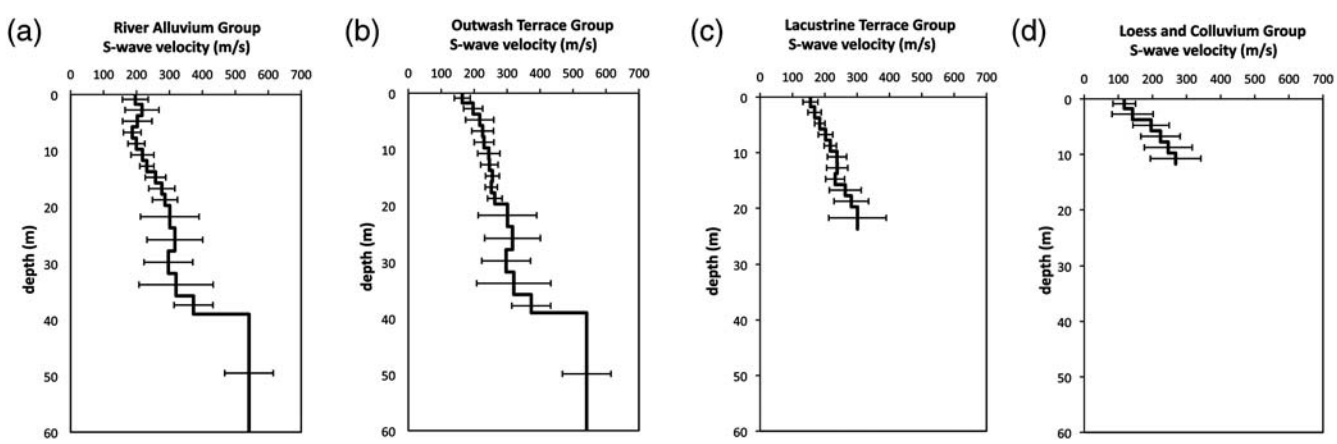

Figure 5. Depth-dependent soil *S*-wave velocity models for (a) river alluvium, (b) outwash terrace, (c) lacustrine terrace, and (d) loess and colluvium groups determined from the CPT and borehole shear-wave velocity profiles. The last measured velocity is extrapolated to the bedrock depth. Error bars show one standard deviation variation in velocities at each depth.

Table 3
Depth-Dependent Shear-Wave Velocities for the River Alluvium, Outwash Terrace, Lacustrine Terrace, and Loess and Colluvium Groups*

River Alluvium Group			Outwash Terrace Group			Lacustrine Terrace Group			Loess and Colluvium Group		
Depth (m)	*S* Velocity (m/s)	Standard Deviation (m/s)	Depth (m)	*S* Velocity (m/s)	Standard Deviation (m/s)	Depth (m)	*S* Velocity (m/s)	Standard Deviation (m/s)	Depth (m)	*S* Velocity (m/s)	Standard Deviation (m/s)
0.00	196.6	39.2	0.00	163.9	24.1	0.00	155.7	23.1	0.00	117.4	33.1
1.75	216.9	51.5	1.75	196.8	28.9	1.75	168.5	20.5	1.75	141.7	60.4
3.75	202.6	44.5	3.75	216.7	42.7	3.75	184.5	16.0	3.75	196.0	53.1
5.75	187.2	26.9	5.75	225.7	32.9	5.75	202.4	22.3	5.75	223.6	57.5
7.75	199.7	25.7	7.75	230.0	29.9	7.75	217.0	19.0	7.75	246.4	70.2
9.75	218.2	34.8	9.75	244.4	33.7	9.75	237.8	29.6	9.75	267.9	73.8
11.75	231.5	21.5	11.75	246.0	26.4	11.75	238.4	32.6	11.75	277.9	64.2
13.75	257.8	31.2	13.75	255.4	21.0	13.75	232.0	29.2	60.00	1251.1	283.5
15.75	277.0	39.5	15.75	251.9	18.4	15.75	263.3	49.2			
17.75	286.5	38.0	17.75	262.7	22.1	17.75	282.0	53.4			
19.75	301.1	88.7	19.75	301.1	88.7	19.75	301.1	88.7			
23.75	316.5	84.7	23.75	316.5	84.7	23.75	316.5	84.7			
27.75	297.0	73.9	27.75	297.0	73.9	27.75	297.0	73.9			
31.75	320.2	112.5	31.75	320.2	112.5	60.00	1251.1	283.5			
35.75	373.2	59.1	35.75	373.2	59.1						
39.00	541.6	73.6	39.75	541.6	73.6						
60.00	1251.1	283.5	60.00	1251.1	283.5						

*Depth to the top of the layer is given.

site-amplification factors are calculated that indicate how bedrock ground motions are amplified or deamplified depending on the soil conditions, as well as the uncertainty in that amplification. A similar approach is taken in this study.

For the actual amplification calculation, we use a one-dimensional (1D) frequency domain approach, assuming shear waves incident on the bedrock/soil interface propagating vertically in a one-dimensionally varying medium (SHAKE91; Idriss and Sun, 1992). It takes into account nonlinear behavior of the soil column using an iterative equivalent linear elastic method. The code has been modified to double the standard precision of the calculations so that soil response is properly calculated at high levels of ground motion above 0.2–0.3g (Cramer, 2006).

The site-amplification factors have some uncertainty because they are calculated based on soil properties and bedrock depth that also have some uncertainty. For the amplification calculation, the interpolated bedrock depth raster was sampled at 0.01° intervals, and the appropriate uncertainty was assigned to the depth depending on whether the point falls in the uplands or lowlands. For each of these points, the predominant geologic unit present at the surface for that cell was used to select the appropriate reference shear-wave velocity profile in Table 3. The bedrock depth was used to select the depth at which to truncate the reference model profile. One hundred realizations of this 1D soil profile were generated that have the distribution of shear-wave velocities and soil layer thicknesses that are found in the measured profiles. Generic values for the dynamic soil properties (shear modulus reduction curves and damping curves) were assumed to be those represented by the Electric Power Research Institute (EPRI, 1993) for sands, depending on the depth range, and by Vucetic and Dobry (1991) for clays. The set of realizations also introduces variations from these average modulus reduction curves and damping curves with a natural lognormal standard deviation of 0.35 (EPRI, 1993). Random variation is introduced into the scaled input bedrock ground motion used in each realization by selecting from a set of 16 ground motions for each realization (Table 4). The 16 input ground-motion recordings come from the Pacific Earthquake Engineering Research (PEER) strong ground-motion database (see Data and Resources). The 100 realizations are used as input to the site response calculation to create a distribution of possible site-amplification factors at each site for each frequency and for 12 different levels of input ground motion, from 0.01–1.0g, at the bedrock interface. At each frequency, the site-amplification distribution is calculated separately with input seismograms scaled to a given response spectral level at that frequency. For example, for the amplification calculation at 0.2-s period and a 0.05 input ground-motion level, the site response is computed using input ground motions scaled to 0.05g in response to spectral amplitude at a 0.2-s spectral acceleration. There is no approximation made to scale a 0.2-s value using a standard response spectral shape, which would require further corrections that are not needed if the response is scaled directly at the frequency of interest. The scaling at specific frequencies also makes the calculation less sensitive to differences in input spectral shape between earthquakes selected in Table 4 and spectra for large earthquakes in the eastern U.S. Inclusion of synthetic ground motions calculated for the eastern U.S. in Table 4 also help account for these differences in the distribution of amplification factors. The median and lognormal standard deviation of the amplification

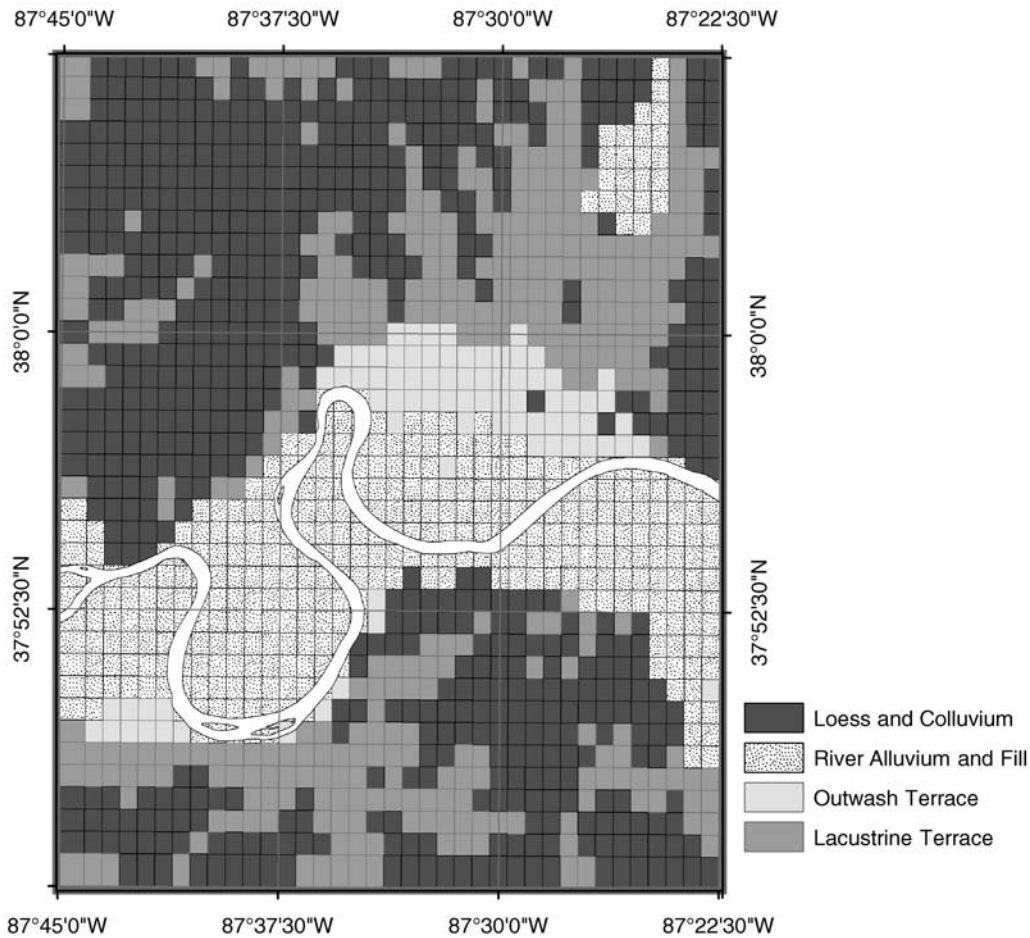

Figure 6. Assignment of velocity profile characteristics at 1-km grid cells based on the geologic unit with the predominant surface area within the cell.

factors are tabulated at each input ground-motion level. Maps of the amplification factor are presented in Figure 9 for selected input ground motion levels. Differences seen in the maps for input ground-motion levels of 0.05g, 0.2g, and 0.5g illustrate the nonlinearity produced by the modification of the shear modulus at high strains. There is a clear correlation with soil depth in the resulting maps.

The amplification for PGA is high outside the limits of the subsurface bedrock valley. The greatest amplification is a factor of 3.25. The smallest amplification is seen in the southeastern quadrangle where bedrock is found at or near the surface. The nonlinear response is seen in the decrease in mean PGA amplification over the entire area from a factor of 2.75 for small ground motions to a factor of 1.75 for large ground motions. The amplification at 0.2-s period is greatest around the edges of the uplands, where depths corresponding to resonant frequencies of 0.2–0.3 s are seen in the resonant period map (Fig. 8). Amplification factors are greater than 4.5 in these areas for small input ground motions. Average amplification decreases from 2.9 to 1.5 with increasing input ground motion due to nonlinear response. For 1.0-s period, strong amplification occurs within the limits of the steep-sided ancient bedrock valley beneath the Ohio River floodplain. There is a large change in amplification factor in the bedrock valley, from 3.5 to 2.1, as input ground motions increase. The overall patterns seen in the amplification at different periods are consistent with the approximate resonant period calculated for the bedrock depth model. Amplification will have a large effect on the probabilistic seismic hazard.

We examined the sensitivity of the amplification factors to the accuracy of the reference model compared to the sensitivity of the amplification factors due to the input ground-motion time histories. Because the overall variations in shear-wave velocity among the four profile types are on the same order as the uncertainties, we would expect that the accuracy of the velocity model would not be very critical. We compared the response for the depth-dependent reference model with several of the individual CPT profiles that were used to calculate the reference model. For small (0.001–0.01g) input ground-motion levels, the response was quite similar in both amplitude and period for the reference model and the individual CPT profiles regardless of the input ground-motion characteristics. For large input ground-motion levels, the variations in response for one reference profile for the range of input ground motions were much larger than the variations in response for the individual CPT

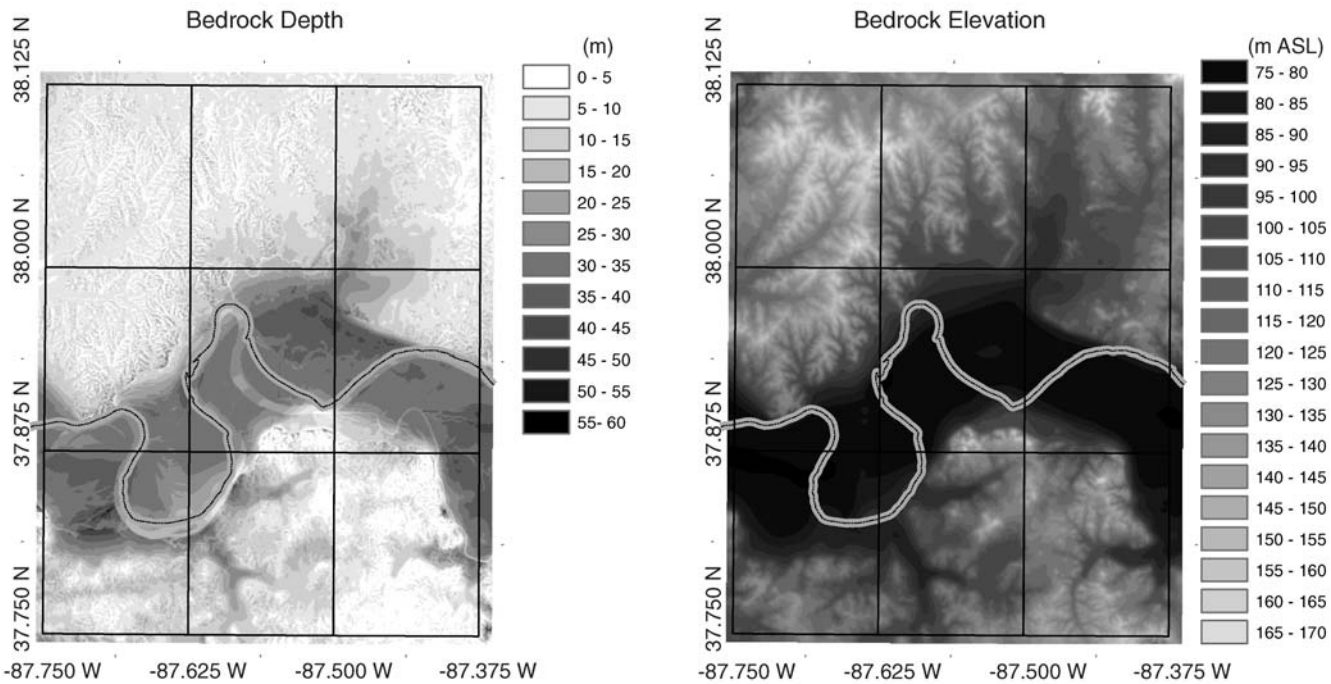

Figure 7. Left: Contoured bedrock depth (meters). Right: contoured bedrock elevation (meters ASL). The steep-sided ancient bedrock valley is evident in both maps beneath the floodplain of the present-day meandering Ohio River.

profiles for a single input ground motion, although the fundamental resonant period did not vary significantly. The strong dependence on the ground-motion record illustrates why it is important to use several ground motions to evaluate the site response, and this was the motivation for selecting a large sample of 16 different ground motions to account for this uncertainty in the resulting amplification factors.

The bedrock model that has been developed has a relatively steep-sided bedrock valley underlying the Ohio River and associated floodplain. Because the resulting amplification maps show a strong dependence on the soil thickness at the edges of this bedrock valley, future work should address the extent to which the 3D geometry affects soil response. Calculating the 1D response using laterally varying 1D soil profiles using SHAKE91 has been applied in this type of study in other areas, such as Charleston, South Carolina (Silva *et al.*, 2003; Chapman *et al.*, 2006); St. Louis, Missouri (Williams *et al.*, 2007); Memphis, Tennessee (Cramer *et al.*, 2004; Cramer, 2006); and in the St. Lawrence River valley near Ottawa, Canada (Benjumea *et al.*, 2008; Motazedian and Hunter, 2008). However, it may not fully capture the 3D response near the bedrock valley edges in the Evansville area. Now that a 3D velocity depth model has been developed, this region is a strong candidate for further study using a 3D site response calculation method to investigate possible basin effects; however, that is beyond the scope of the present study. The effects of liquefaction, complex nonrandom variations in V_S within a region that we treat with random variations from a single reference profile, and more complex variations in bedrock velocity could also affect the true response at a site. Future work should also focus on the collection and analysis of additional seismic data in order to validate the

Table 4
Suite of Input Bedrock Ground Motions Used in Site Response Calculation

Event	Date (yyyy-mm-dd)	M_w	Site	Components
Cape Mendocino	1992-04-25	7.0	CPM (CDMG 89005) Cape Mendocino	N, E
Kobe	1995-01-16	6.9	KJMA	N, E
Landers	1992-06-28	7.3	JOS Joshua Tree	N, E
Duzce	1999-11-12	7.1	1060	N, E
Kocaeli	1999-08-17	7.4	GBZ	W
Kocaeli	1999-08-17	7.4	IZT	S
Loma Prieta	1989-10-18	6.9	47379 Gilroy Array #1	N, E
Chi-Chi	1999-09-20	7.6	TCU046	N, W
Simulated*		7.5		horizontal
Simulated*		8.0		horizontal

*Beresnev and Atkinson (2002).

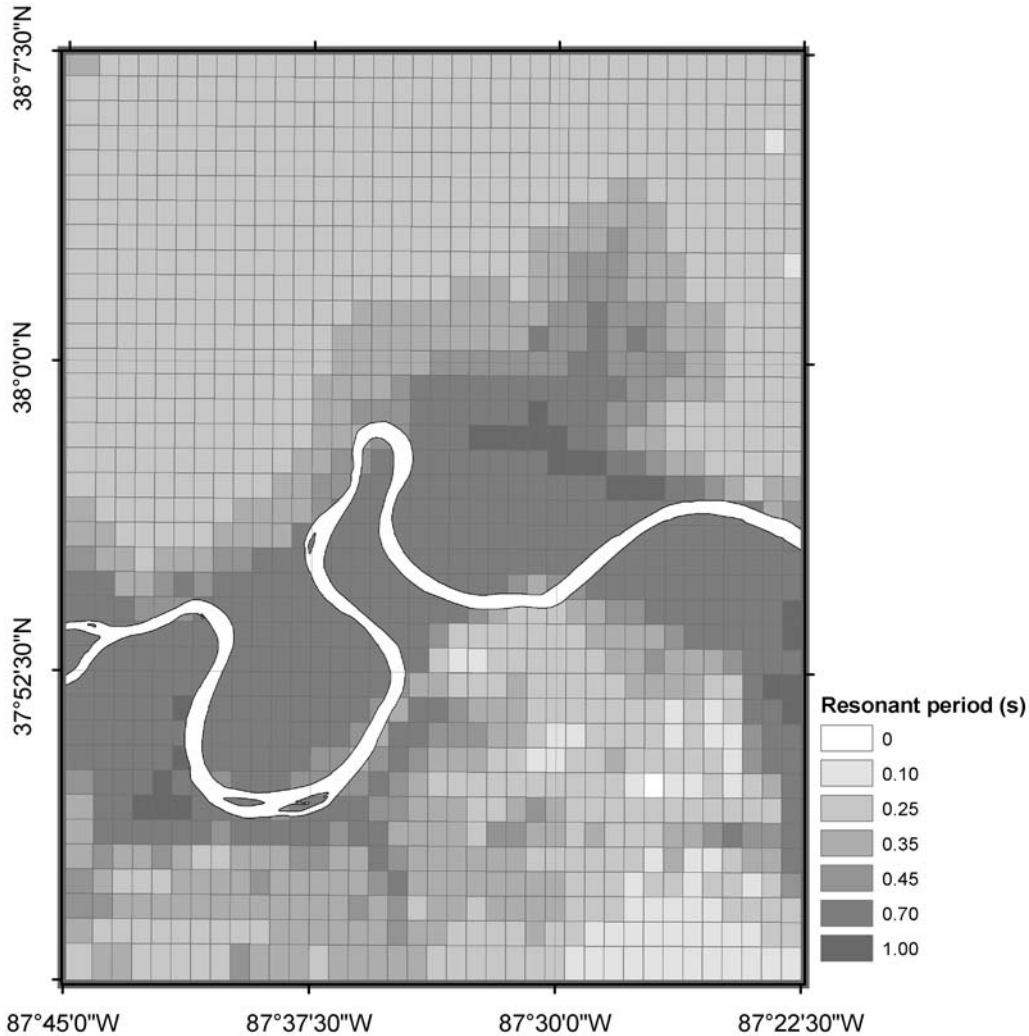

Figure 8. Resonant period assuming linearity, calculated as $T = 4d/V_S$.

amplifications calculated with the model, especially at locations where infrastructure and population are most likely to be affected. A recent study of the 2008 M_w 5.4 Mt. Carmel earthquake in Illinois showed site resonances of 0.1 s and 0.5 s for USIN and EVIN, two seismic stations found within the study area (Odum *et al.*, 2010). This is at the lower end of the range of uncertainty for the site resonant periods calculated using the quarter-wavelength approximation for these two sites. The approximate resonant period calculated using the model derived in this study is 0.1–0.3 s for site USIN and 0.4–0.6 for EVIN. Earthquake sources like these are rare, so methods that use a horizontal-to-vertical ratio of noise recordings, for example, are another way that the lateral variation of response could be tested more thoroughly, at least for lower input ground-motion levels.

Probabilistic Seismic-Hazard Calculation and Results

The amplification factors computed in the previous section are incorporated into the calculation of the probabilistic seismic hazard in the following manner. When constructing the hazard curve for an individual point in the map area, the probability of a given source producing shaking at the site is calculated in the same way as described in the previous section for the national seismic-hazard maps, except for the use of the attenuation curves. When calculating the probable level of ground motion appropriate for the source size and distance, a modified attenuation relation is used. The attenuation relations in Table 1 are modified based on the amplification factor distribution for the site of interest to provide new attenuation relations valid for a soil site with modified uncertainties (Cramer, 2003). These modified attenuation relations are used to construct the hazard curve for the site that gives the probability of a certain ground-motion level being exceeded, given the probability of occurrence of each seismic source. The ground motion corresponding to a prescribed probability level of exceedance is selected from the hazard curve at each site to make the final PSHA that now includes the site amplification and its associated uncertainties.

The probabilistic seismic-hazard maps have been computed for PGA and spectral acceleration at 0.1-, 0.2-, 0.3-,

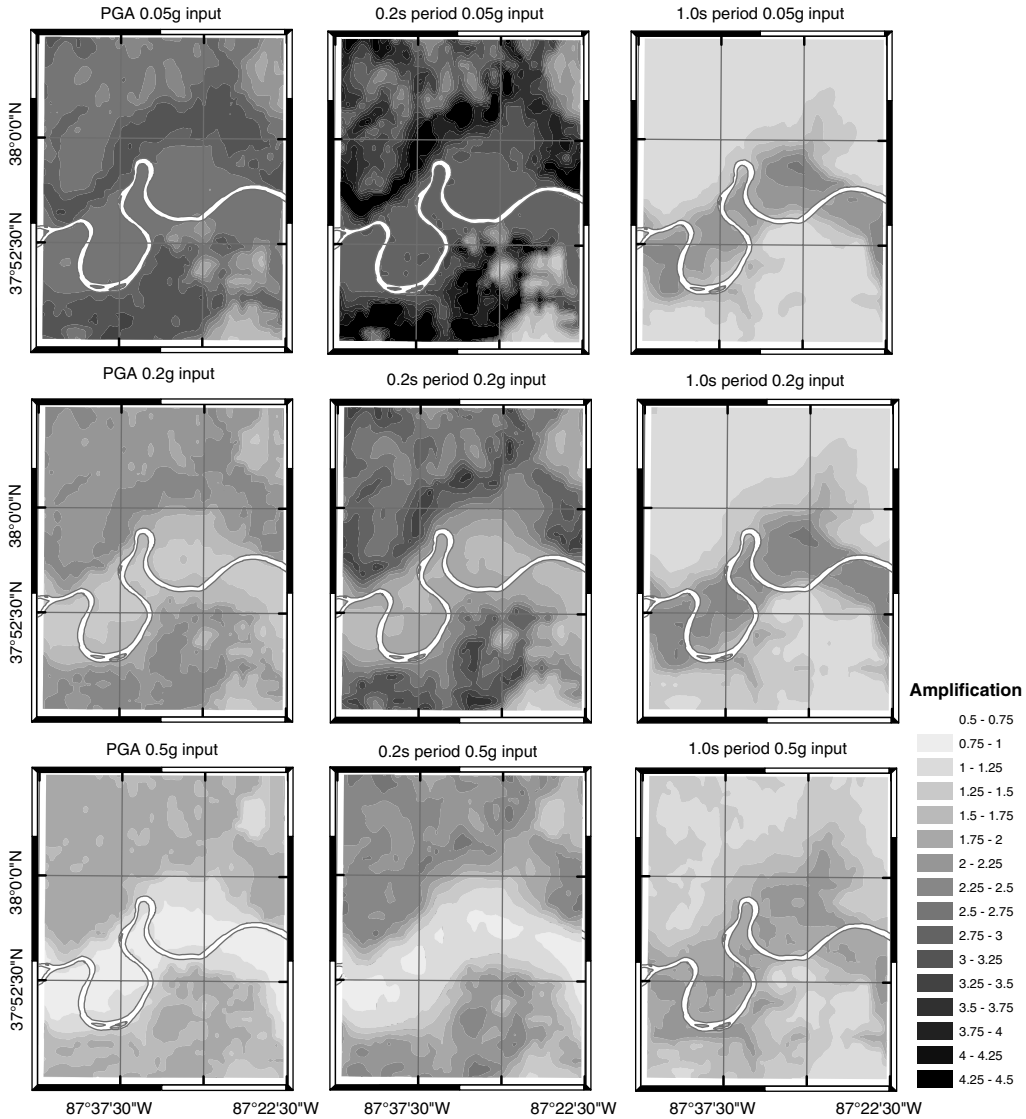

Figure 9. Results of the calculation of site-amplification relative to input bedrock ground motion. Top row is PGA amplification, middle row is amplification at 0.2 s spectral acceleration, lower row is amplification at 1.0 s.

0.5-, 1.0-, and 2.0-s periods with 2%, 5%, and 10% PE in 50 yr. The 2% maps for PGA, 0.2-s, and 1.0-s periods are presented here (Fig. 10). PGA values of 0.5–0.6g are found uniformly across the northwestern and southwestern parts of the map area, corresponding to shallow bedrock areas. The 0.2-s spectral acceleration reaches 1.3–1.5g north and south of the Ohio River valley where soils are 10–15 m thick. At 1.0-s period, the higher accelerations of 0.3–0.45g are strictly limited to the ancient bedrock valley beneath the floodplain and major ancient bedrock tributaries leading into the main valley.

By considering the effect of local site conditions on ground motions, the probabilistic seismic-hazard analysis overall raises the estimates of acceleration with 2% probability of being exceeded in 50 yr when compared with the USGS 2008 national seismic-hazard maps, with certain exceptions. The PGA ranges from 0.3–0.7g, compared with the values of approximately 0.3g provided in the national maps, which assume NEHRP class B/C conditions with a 30-m averaged shear-wave velocity of 760 m/s. The PSHA 0.2-s spectral accelerations range from 0.7–1.5g for the uplands areas and terraces with shallow-to-moderate depth sediments, compared with 0.5–0.7g in the national maps. On the other hand, within the ancient bedrock valley beneath the floodplain, spectral accelerations are comparable to the national map values of 0.5–0.7g. The PSHA 1.0-s spectral accelerations are as high as 0.45g within the limits of this ancient bedrock valley, but range from 0.1 to 0.2g outside that area where values are comparable to the national map values.

Because the soil types of the Evansville area have characteristics typical of NEHRP class D site conditions (V_S less than 360 m/s) at the surface, it is relevant to compare the high-resolution PSHA results that include site amplification to the national map values with a uniform site D amplification factor applied (Building Seismic Safety Council, 2003;

Fig. 10). The high-resolution PSHA maps for PGA with completely probabilistic treatment of site effects, can then be seen to have significantly larger accelerations than those provided in the national maps with NEHRP class D conditions in almost all areas aside from the ancient bedrock valley. The high-resolution PSHA map for 0.2-s spectral accelerations shows much higher values than the 0.6–0.8g values of the USGS 2008 national maps with site D conditions, except within the ancient bedrock valley where 0.8g in the national maps is lowered to 0.6g with the probabilistic site conditions. The PSHA 1.0-s spectral accelerations, when including site effects, are seen to be comparable to the national map values with D site conditions for most of the area within the limits of the ancient bedrock valley, but are significantly lower outside those limits. Several factors contribute to these differences. First, while materials at the surface appear to have class

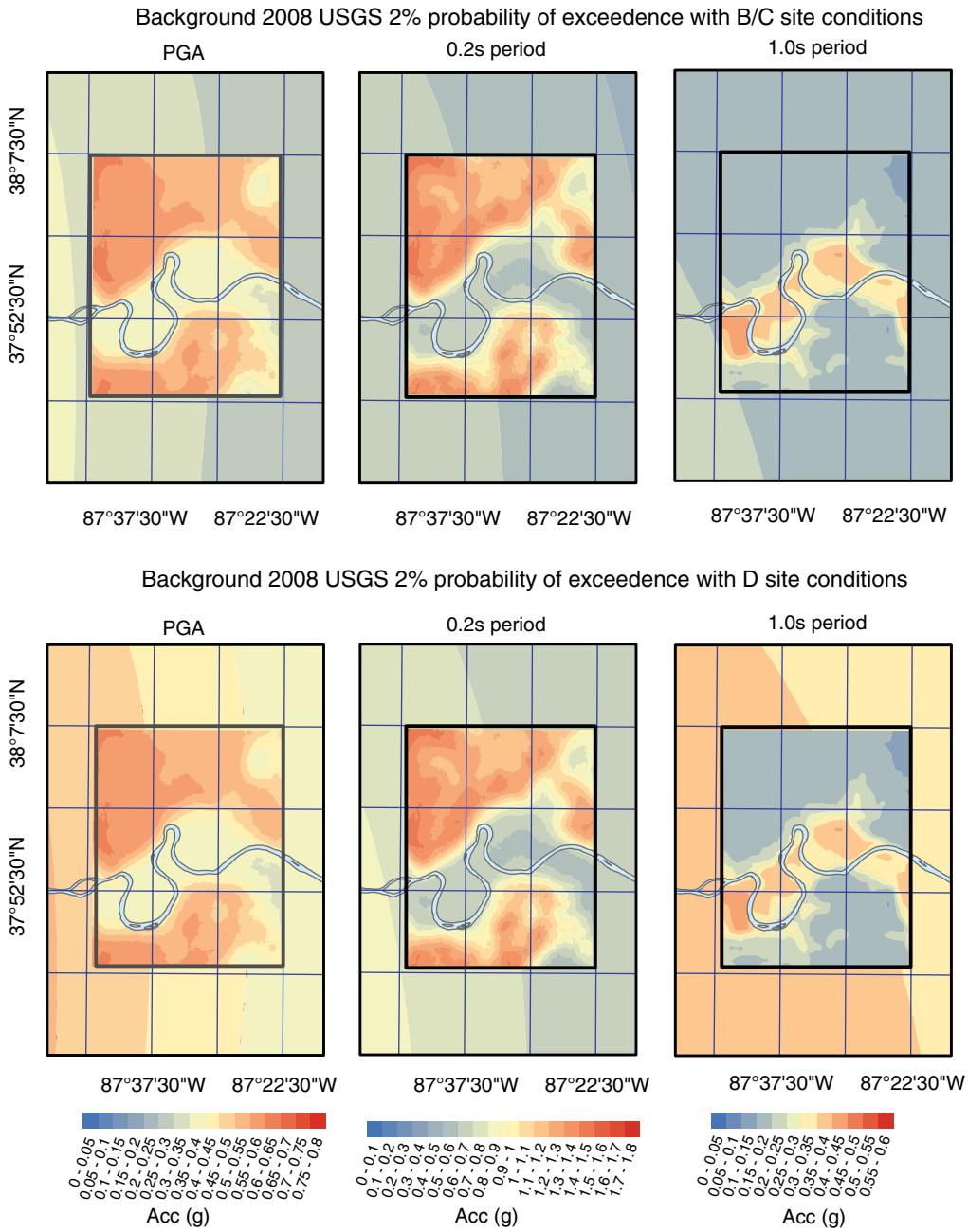

Figure 10. Upper left: Inset shows PGA level with 2% probability of being exceeded in 50 yr from the high-resolution probabilistic calculation including site effects. Background shows the USGS 2008 national map values for NEHRP site class B/C. Upper center: the same as the upper left for 0.2-s spectral acceleration. Upper right: the same as the upper left for 1.0-s spectral acceleration. Lower left: Inset shows PGA level with 2% probability of being exceeded in 50 yr from the high-resolution probabilistic calculation including site effects. Background shows the USGS 2008 national map values for NEHRP site class D. Lower center: the same as the lower left for 0.2-s spectral acceleration. Lower right: the same as the lower left for 1.0-s spectral acceleration. All plots are in units of acceleration (g).

D–type seismic velocities, the thickness varies, and in particular, thinner soils (< 25 m) surrounding the Ohio River valley will not have resonances near 1.0 s. Second, the NEHRP amplification factors are derived from data outside the CEUS. Third, nonlinearity for large input ground motions appears to be important in limiting the maximum accelerations. This results from shear-wave modulus reduction and damping curves iteratively applied in the site-response calculation. The modulus reduction curves and damping curves are based on generic soil properties. Given that they have a significant impact on the final result, it suggests that more work should be aimed at improving our knowledge with *in situ* measurements of these properties.

The impact of site effects on seismic hazard has been investigated in several areas in the CEUS with exposure to hazard from historic source zones: Charleston, South Carolina (Silva *et al.*, 2003; Chapman *et al.*, 2006); St. Louis, Missouri (Williams *et al.*, 2007); Memphis, Tennessee (Cramer *et al.*, 2004; Cramer, 2006); and in the St. Lawrence River valley near Ottawa, Canada (Benjumea *et al.*, 2008; Motazedian and Hunter, 2008). These locations have similar near-surface fluvial depositional characteristics, with similar seismic velocities measured in the 100–300 m/s range near the surface. Data collected in these regions also lead to partitioning into upland areas with some low-topographic relief and with relatively shallow soils (< 20 m) and flatter alluvial areas with thicker soil units (> 30–40 m) based on geotechnical measurements. Similar results were found among these studies in terms of significant amplification occurring in upland areas with thinner sediments at 0.2–0.4 s and amplification occurring in the lowlands with periods > 0.8 s. This effect is dramatic in the Evansville area because of the steepness of the bedrock topography. On the other hand, Charleston and Memphis have deep sequences of Tertiary and Cretaceous units forming large-scale basin structures with V_S in the 600–1200 m/s range and approximately 600–1200 m thick before reaching bedrock in addition to shallow low-velocity unconsolidated soil layers. The effects of the near-surface units and the Tertiary/Cretaceous units were investigated separately in Chapman *et al.* (2006). Both the Memphis and Charleston study areas have amplification factors on the order of 3 at 1.0-s period throughout the study region regardless of the presence of the low-velocity soils near the surface layers. For near-surface response, general similarity among these studies provides some support to the approach of using high-resolution topography as a proxy for V_{S30} (Allen and Wald, 2009), when thick Tertiary/Cretaceous sequences are not present. The steep bedrock valley walls in the Evansville area create a very clear spatial signature that is quite different at 0.2-s and 1.0-s periods, compared with other study areas. The Evansville area is a strong candidate for further study using a 3D site response calculation method because the current calculation was based on a 1D spectral approach that will likely have limited accuracy near the valley edges.

Conclusions

Detailed geologic mapping and comprehensive CPT sampling of soil profiles in the Evansville region now make it possible to estimate site amplification and its uncertainty with a high level of detail. The unique depositional history of the soils in the region creates several distinct soil profile types, each of which has been characterized statistically in this study. The amplification patterns that emerge at all frequencies are strongly controlled by depth to bedrock. The distributions of the amplification factors (median and log standard deviation) have been characterized at each 0.01° grid point within the region by calculating site response with 100 realizations of the soil profile properties. The distributions of amplification factors have then been used in a completely probabilistic methodology for including site effects in the probabilistic hazard calculation. The resulting PSHA maps of acceleration with 2% probability of exceedance in 50 yr show patterns with strong local variations, and these maps locally exceed the national seismic-hazard map values with B/C site conditions. When compared to the national maps with a uniform site D class amplification factor applied, there are large local differences between the national maps and the high-resolution PSHA maps at all periods, which illustrates the importance of using a high-resolution seismic-hazard analysis in this type of environment.

This study illustrates that at distances from 150–350 km from a major seismic-hazard zone like New Madrid, the variations in hazard values due to local site effects can be more important than variations in hazard values due to proximity to potential seismic sources. Similar urban seismic-hazard assessments should be encouraged to promote seismic-hazard mitigation for land planning and zoning at the local level in other areas where distant seismic sources are of concern.

Data and Resources

CPT data were taken from the USGS CPT Data for Evansville, Indiana, Area, collected by T.L. Holzer and the USGS Western Earthquake Hazards Team in 2003 and 2004 and can be obtained at http://earthquake.usgs.gov/regional/nca/cpt/data/?map=evansville (last accessed September 2009).

Ground-motion recordings are from the PEER strong ground-motion database, available at http://peer.berkeley.edu/smcat/ (last accessed September 2009).

S-wave refraction profiles are available in Bauer and CUSEC (2005). Images can be obtained at the following web site: http://earthquake.usgs.gov/research/external/reports/01HQGR0195.pdf (last accessed September, 2009).

The SPT blow count data are available by request to the Indiana Geological Survey in Bloomington, Indiana.

The *P*-wave refraction data are available online at the following web site: http://inmap.indiana.edu/dload_page/geology.html (last accessed September 2009)

The iLITH GIS water well log database, along with the report, and ArcView plotting tools are available in Brown *et al.* (2008).

The bedrock depth data from oil, gas, and water well logs in Kentucky are archived at the Kentucky Geological Survey and can be obtained by request to the Kentucky Geological Survey, Henderson, Kentucky.

The Geographic Information System files containing the velocity and bedrock depth models, amplification results, and PSHA maps will be made available electronically at the Indiana Geological Survey http://www.igs.indiana.edu/arcims/index.cfm.

Acknowledgments

This work was supported by USGS NEHRP Awards 05HQGR0033 and 07HQGR0058. The surficial geologic mapping was carried out as part of the Evansville Area Earthquake Hazards Mapping Project. We would like to acknowledge the contribution to the mapping from Ronald C. Counts, Steven L. Martin, Michael L. Murphy, Mark F. Thompson, and William "Drew" Andrews of the Kentucky Geological Survey and Dave Moore and Scott Lundstrom of the USGS. We thank Robert Bauer of the Illinois State Geological Survey, John Hill of the Indiana Geological Survey, Oliver Boyd of the USGS, and Chris Cramer from the University of Memphis for their constructive review of this work. We would like to thank Tom Holzer, Thomas Noce, and the USGS for collecting and making available the new high-quality CPT observations in the area. We thank Josh Messmer for assistance with figure preparation for this article. Access to point data and other databases was greatly facilitated by access through GIS databases maintained by the IGS. We acknowledge the efforts of Joan Gomberg, Eugene "Buddy" Schweig, and Oliver Boyd of the USGS, Jim Cobb, John Kiefer, and Dave Williams of the KGS, John Steinmetz of the IGS, and Christine Martin of the Southwest Indiana Disaster Resistant Community Corporation for providing continuing interest in the results of the group effort to create the seismic-hazard maps. We especially thank Chris Cramer for his advice and consultation for implementing the probabilistic site effects in the seismic-hazard calculation. We thank Michael Hamburger, Steve Harmsen, Charles Mueller, and an anonymous reviewer for their constructive comments on this work.

References

Allen, T. L., and D. J. Wald (2009). On the use of high-resolution topographic data as a proxy for seismic site conditions (V_{S30}), *Bull. Seismol. Soc. Am.* **99,** no. 2A, 935–943.

Atkinson, G., and D. M. Boore (2006). Earthquake ground-motion prediction equations for eastern North America, *Bull. Seismol. Soc. Am.* **96,** no. 6, 2181–2205.

Bakun, W. H., and M. G. Hopper (2004). Magnitudes and locations of the 1811–1212 New Madrid, Missouri, and the 1886 Charleston, South Carolina, earthquakes, *Bull. Seismol. Soc. Am.* **94,** no. 1, 64–75.

Bauer, R. A., and CUSEC (2005). Central U.S. shear wave velocity database with accompanying geological/geotechnical information of nonlithified geologic materials, U.S. Geol. Surv. External Res. Prog. Final Rept. 04HQGR0074, Central United States Earthquake Consortium, 29 pp., available at http://earthquake.usgs.gov/research/external/reports/01HQGR0195.pdf.

Benjumea, B., J. A. Hunter, S. E. Pullan, G. R. Brooks, M. Pyne, and J. M. Aylsworth (2008). $V_{S(30)}$ and fundamental site period estimates in soft sediments of the Ottawa Valley from near-surface geophysical measurements, *J. Environ. Eng. Geophys.* **13,** no. 4, 313–323.

Beresnev, I. A., and G. Atkinson (2002). Source parameters of earthquakes in eastern and western North America based on finite-fault modeling, *Bull. Seismol. Soc. Am.* **92,** no. 2, 660–682.

Bleuer, N. K. (2000). *iLITH database of the Indiana Geological Survey*, Indiana Geological Survey, Bloomington, Indiana.

Brown, S.E., N.K. Bleuer, M. O'Neal, J. Olejnik, and R. Rupp (2008). Glacial Terrain Explorer, Geological Survey Open-File Study 00-08, CD-ROM.

Building Seismic Safety Council (2003). *National Earthquake Hazards Reduction Program Recommended Provisions and Commentary for Seismic Regulations for New Buildings and Other Structures (FEMA 450), Part 1: Provisions*, Federal Emergency Management Agency, Washington, D.C., 356 pp.

Calais, E., and S. Stein (2009). Time-variable deformation in the New Madrid Seismic Zone, *Science* **323,** no. 5920, 1442–1442.

Campbell, K. W., and Y. Bozorgnia (2003). Updated near-source ground-motion (attenuation) relations for the horizontal and vertical components of peak ground acceleration and acceleration response spectra, *Bull. Seismol. Soc. Am.* **93,** no. 1, 314–331.

Central United States Earthquake Consortium (CUSEC) (2004). *Central U.S. shear wave velocity database with accompanying geological/geotechnical information of nonlithified geologic materials*, 29 pp.

Chapman, M. C., J. R. Martin, C. G. Olgun, and J. N. Beale (2006). Site-response models for Charleston, South Carolina, and vicinity developed from shallow geotechnical investigations, *Bull. Seismol. Soc. Am.* **96,** no. 2, 467–489.

Cramer, C. H. (2003). Site specific seismic hazard analysis that is completely probabilistic, *Bull. Seismol. Soc. Am.* **93,** no. 4, 1841–1846.

Cramer, C. H. (2006). Quantifying the uncertainty in site amplification modeling and its effects on site-specific seismic hazard estimation in the upper Mississippi embayment and adjacent areas, *Bull. Seismol. Soc. Am.* **96,** no. 6, 2008–2020.

Cramer, C., J. S. Gomberg, E. S. Schweig, B. A. Waldron, and K. Tucker (2004). *The Memphis, Shelby County, Tennessee, seismic hazard maps*, 46 pp, Memphis, Tennessee.

Eggert, D. L., A. C. Samuelson, J. D. Bray, C. W. Chang, W. R. Eckhoff, K. Kayabali, E. J. McClees, T. R. West, M. C. Woodfield, and B. Zheng (1994). *Final report to the city of Evansville: Shear-wave and earthquake hazard mapping of Evansville, Indiana*, 17 pp, Indiana Geological Survey, Bloomington, Indiana.

Eggert, D. L., M. C. Woodfield, N. K. Bleuer, and E. J. Hartke (1996). *Geologic terrain map of the Indiana portion of the Newburgh quadrangle, Indiana-Kentucky*, Indiana Geological Survey, Bloomington, Indiana.

Eggert, D. L., M. C. Woodfield, N. K. Bleuer, and E. J. Hartke (1997a). *Geologic terrain map of the Evansville region, Indiana*, Indiana Geological Survey, Bloomington, Indiana.

Eggert, D. L., M. C. Woodfield, N. K. Bleuer, and E. J. Hartke (1997b). *Geologic terrain map of the Daylight quadrangle*, Indiana Geological Survey, Bloomington, Indiana.

EPRI (1993). *Guidelines for determining design basis ground motions*, vol. **1–5**, no. TR-102293, Electric Power Research Institute, Palo Alto, California.

Frankel, A., C. Mueller, T. Barnhard, D. Perkins, E. V. Leyendecker, N. Dickman, S. Hanson, and M. Hopper (1996). *National seismic hazard maps: Documentation June 1996*, 110 pp.

Frankel, A., M. Petersen, C. Mueller, K. Haller, R. Wheeler, E. V. Leyendecker, R. Wesson, S. Harmsen, C. Cramer, D. Perkins, and K. Rukstales (2002). *Documentation for the 2002 update of the national seismic hazard maps*, 33 pp.

Gray, H. H. (1983). Map of Indiana showing thickness of unconsolidated deposits, *Miscellaneous Map 37*, Indiana Geological Survey, Bloomington, Indiana, scale 1:500,000.

Gray, H. H. (1989). Quaternary geologic map of Indiana, *Miscellaneous Map 49*, Indiana Geological Survey, Bloomington, Indiana, scale 1:500,000.

Green, R. A., S. F. Obermeier, and S. M. Olson (2005). Engineering geologic and geotechnical analysis of paleoseismic shaking using liquefaction effects: Field examples, *Eng. Geol.* **76,** 263–293.

Holzer, T. L. (2003). Earthquake Hazards: USGS CPT Data: Evansville Indiana Area, available at http://quake.wr.usgs.gov/prepare/cpt/, United States Geological Survey.

Hough, S., J. G. Armbruster, L. Seeber, and J. F. Hough (2000). On the modified Mercalli intensities and magnitudes of the 1811–1812 New Madrid earthquakes, *J. Geophys. Res. (Solid Earth)* **105,** no. B10, 23,839–23,864.

Idriss, I. M., and J. I. Sun (1992). *User's manual for SHAKE91*, Center for Geotechnical Modeling, Dept. of Civil and Environmental Engineering, University of California, Davis, California.

Johnston, A. C.. (1996). Seismic moment assessment of earthquakes in stable continental regions: II. New Madrid 1811–1812, Charleston 1886 and Lisbon 1755, *Geophy. Int. J.* **126,** no. 2, 314–344.

Kramer, S. L. (1996). *Geotechnical Earthquake Engineering*, 653 pp., Prentice Hall, New Jersey.

McGuire, R. K. (2004). *Seismic Hazard and Risk Analysis*, Earthquake Engineering Research Institute, Oakland, California, 221 pp.

McNulty, W. E., and S. F. Obermeier (1999). Liquefaction evidence for at least two strong Holocene paleo-earthquakes in central and southwestern Illinois, USA, *Environ. Eng. Geosci.* **5,** no. 2, 133–146.

Moore, D. W., S. C. Lundstrom, R. C. Counts, S. L. Martin, W. M. Andrews Jr., W. L. Newell, M. L. Murphy, M. F. Thompson, E. M. Taylor, E. P. Kvale, and T. R. Brandt (2009), Surficial geologic map of the Evansville, Indiana and Henderson, Kentucky area, Denver, Colorado, scale 1:50,000.

Motazedian, D., and J. Hunter (2008). Development of an NEHRP map for the Orleans suburb of Ottawa, Ontario, *Canadian Geotech. J.* **45,** no. 8, 1180–1188.

Munson, P. J., C. A. Munson, and E. C. Pond (1995). Paleoliquefaction evidence for a strong holocene earthquake in south-central Indiana, *Geology* **23,** no. 4, 325–328.

Munson, P. J., and C. A. Munson (1996). *Paleoliquefaction evidence for recurrent strong earthquakes since 20 000 yr B.P. in the Wabash Valley area of Indiana*, Indiana University, Bloomington, Indiana, 137 pp.

Nuttli, O. W. (1973). The Mississippi Valley earthquakes of 1811 and 1812: Intensities, ground motion and magnitudes, *Bull. Seismol. Soc. Am.* **63,** no. 1, 227–248.

Odum, J. K., W. J. Stephenson, and R. A. Williams (2010). Predicted and observed spectral response from collocated shallow, active- and passive-source V_S data at five ANSS sites, Illinois and Indiana, USA, *Seismol. Res. Lett.* **81,** no. 6, 955–964.

Olson, S. M., R. A. Green, and S. F. Obermeier (2005). Revised magnitude-bound relation for the Wabash Valley Seismic Zone of the central United States, *Seismol. Res. Lett.* **76,** no. 6, 756–771.

Petersen, M. D., A. D. Frankel, S. C. Harmsen, C. S. Mueller, K. M. Haller, R. L. Wheeler, R. L. Wesson, Y. H. Zeng, O. S. Boyd, D. M. Perkins, N. Luco, E. Field, C. J. Wills, and K. S. Rukstales (2008). *Documentation for the 2008 update of the national seismic hazard maps*, 60 pp.

Pond, E. C. (1996). *Seismic parameters for the central United States based on paleoliquefaction evidence in the Wabash Valley*, *Ph.D. Thesis*, Virginia Polytechnic Institute, Blacksburg, Virginia.

Richter, C. F. (1958). *Elementary Seismology*, W. H. Freeman & Co., New York.

Rudman, A. J., M. E. Biggs, R. F. Blakely, and J. F. Whaley (1973). Statistical studies of Indiana bedrock velocities: Mapping applications, *Indiana Academy of Science* **83,** no. 1973, 284–290.

Silva, W., N. Gregor, and R. Darragh (2002). *Development of hard rock attenuation relations for central and eastern North America*, 27 pp, Pacific Engineering, El Cerrito, California.

Silva, W., I. Wong, T. Siegel, N. Gregor, R. Darragh, and R. Lee (2003). Ground motion and liquefaction simulation of the 1886 Charleston, South Carolina, earthquake, *Bull. Seismol. Soc. Am.* **93,** no. 6, 2717–2736.

Somerville, P. G., N. N. Collins, N. Abrahamson, R. Graves, and C. Saikia (2001). *Ground motion attenuation relations for the Central and Eastern United States*, 38 pp.

Street, R. (1984). *The Historical Seismicity of the Central United States: 1811–1928*, Dept. of Geology, University of Kentucky, Lexington, Kentucky,316 pp.

Tavakoli, B., and S. Pezeshk (2005). Empirical-stochastic ground-motion prediction for eastern North America, *Bull. Seismol. Soc. Am.* **95,** no. 6, 2283–2296.

Toro, G. R., N. A. Abrahamson, and J. F. Schneider (1997). Model of strong ground motions from earthquakes in central and eastern North America: Best estimates and uncertainties, *Seismol. Res. Lett.* **68,** no. 1, 41–57.

Tuttle, M. P., E. S. Schweig, J. D. Sims, R. H. Lafferty, L. W. Wolf, and M. L. Haynes (2002). The earthquake potential of the New Madrid Seismic Zone, *Bull. Seismol. Soc. Am.* **92,** no. 6, 2080–2089.

Tuttle, M. P., E. S. Schweig, J. Cambell, P. J. Thomas, J. D. Sims, and R. H. Lafferty (2005). Evidence for New Madrid earthquakes in A.D. 300 and 2350 B.C., *Seismol. Res. Lett.* **76,** no. 4, 489–501.

USGS (2004). 1-arc-second national elevation dataset, available at http://seamless.usgs.gov/products/1arc.php, June 2004.

Vucetic, M., and R. Dobry (1991). Effect of soil plasticity on cyclic response, *J. Geotech. Eng.* **117,** 89–107.

Weichert, D. H. (1980). Estimation of the earthquake recurrence parameters for unequal observation periods for different magnitudes, *Bull. Seismol. Soc. Am.* **70,** no. 4, 1337–1346.

Wheeler, R. L., and C. H. Cramer (2002). Updated seismic hazard in the southern Illinois basin: Geological and geophysical foundations for use in the 2002 USGS National Seismic Hazard Maps, *Seismol. Res. Lett.* **73,** no. 5, 776–791.

Williams, R. A., J. K. Odum, W. J. Stephenson, and R. B. Herrmann (2007). Shallow *P*- and *S*-wave velocities and site resonances in the St. Louis region, Missouri-Illinois, *Earthq. Spectra* **23,** no. 3, 711–726.

Department of Earth & Atmospheric Science
Purdue University
550 Stadium Mall Dr
West Lafayette, Indiana 47907-2051
jhaase@purdue.edu
(J.S.H., T.B., R.L.N.)

School of Civil Engineering
Purdue University
West Lafayette, Indiana
(Y.-S. C.)

Manuscript received 5 October 2009